

# Tuning Superinductors by Quantum Coherence Effects for Enhancing Quantum Computing

Bo Fan,<sup>1,\*</sup> Abhisek Samanta,<sup>2,†</sup> and Antonio M. García-García<sup>1,‡</sup>

<sup>1</sup>*Shanghai Center for Complex Physics, School of Physics and Astronomy,  
Shanghai Jiao Tong University, Shanghai 200240, China*

<sup>2</sup>*Physics Department, Technion, Haifa 32000, Israel*

Research on spatially inhomogeneous weakly-coupled superconductors has recently received a boost of interest because of the experimental observation of a dramatic enhancement of the kinetic inductance with relatively low losses. Here, we study the kinetic inductance and the quality factor of a strongly-disordered weakly-coupled superconducting thin film. We employ a gauge-invariant random-phase approximation capable of describing collective excitations and other fluctuations. In line with the experimental findings, we have found that in the range of frequencies of interest, and for sufficiently low temperatures, an exponential increase of the kinetic inductance with disorder coexists with a still large quality factor  $\sim 10^4$ . More interestingly, on the metallic side of the superconductor-insulator transition, we have identified a range of frequencies and temperatures  $T \sim 0.1T_c$  where quantum coherence effects induce a broad statistical distribution of the quality factor with an average value that increases with disorder. We expect these findings to further stimulate experimental research on the design and optimization of superinductors for a better performance and miniaturization of quantum devices such as qubit circuits and microwave detectors.

A microwave resonator that is both low-loss and small [1–3] is an important element in circuits designed for quantum computation or photon detection. For instance, a high-inductance element [4] suppresses charge fluctuations and slows down electromagnetic waves which increases coherence times and facilitates the circuit miniaturization. Devices such as the fluxonium qubit [5] have a kinetic inductance  $L_{k/\square}$  orders of magnitude larger than the geometrical one related to its shape and it is further enhanced by increasing disorder. For that reason, there have been an explosion of interest [5–19] in disordered superconductors as high-inductance devices, commonly called superinductors. Promising results [9–16] have been reported for nano-wires of NbN<sub>x</sub>, tin, granular Al [20–24] and nano-wires of Al based materials [6–8, 19].

These materials have also drawbacks. The presence of sub-gap collective excitations [25–27], specially the Goldstone mode [28] related to phase fluctuations, in highly disordered superconductors [29–33] may shorten coherence times in superconducting circuits. Another potential problem is the existence of strong losses [34, 35] in amorphous dielectric due to two level systems. Although this source of decoherence can to some extent be controlled, for instance by reducing the device size [34, 35], it can reduce the coherence time of the device. However, the current experimental evidence [11, 14] is that this effect is not dominant.

Quantum coherence effects play an important role in weakly-coupled disordered superconductors. The order parameter becomes highly inhomogeneous [36–44] with a multifractal-like spatial structure close to the insulating transition leading to the enhancement of superconductivity [36]. Level degeneracies [45–48] cause similar effects in granular materials [40, 41] and single superconducting grains. These theoretical findings have been largely confirmed experimentally [20, 49–56].

The above results call for a detailed theoretical study of quantum coherence effects in the kinetic inductance and quality factor of disordered superconducting thin films.

In this paper, we address this problem in a two dimensional weakly-coupled disordered superconductor close to the insulating transition but still on the metallic side. We compute these observables by the mean-field limit of the attractive Hubbard model in the weak-coupling limit, namely, the self-consistent Bogoliubov de-Gennes (BdG) formalism [57, 58]. Corrections to the BdG formalism are obtained by a random phase approximation leading to gauge-invariant results. Diagrammatically, these deviations correspond to vertex corrections to the mean-field bubble-diagrams representing the current-current correlation function. Gauge invariance is necessary in order to reproduce sub-gap collective excitations such as the Goldstone mode [28] that may increase losses dramatically and therefore prevent the use of disordered superconductors as high-inductance devices. We shall see that, in contrast with previous results [59] on the insulating side of the transition, collective excitations do not occur in the region of interest. Moreover, in agreement with experiments, the kinetic inductance increases with disorder without a drastic reduction of the quality factor.

*Kinetic inductance and Quality factor of a superinductor device.*— The reactance is defined as  $X = 2\pi f L_{k/\square}$ , so a high performance superinductor requires a large kinetic inductance  $L_{k/\square}$ . According to the Mattis-Bardeen theory [27], the kinetic inductance of a superconductor is  $L_{k/\square} \sim \frac{\hbar R_{\square}}{\pi \Delta}$ , where  $R_{\square}$  is the sheet resistance of the material and  $\Delta$  is the amplitude of the superconducting order parameter. Therefore,  $L_{k/\square}$  is enhanced by increasing the sheet resistance, which effectively is equivalent to an increase of the disorder strength. However, as mentioned earlier, disorder can also lead to a stronger dissipation at micro-wave frequencies due to collective modes and other fluctuations [30, 32, 33] that induce sub-gap structure in the conductivity near the insulating transition. Therefore, it is important that the enhancement of the kinetic inductance by disorder is not accompanied by these dissipative effects.

Dissipation effects are described by the quality factor  $Q =$

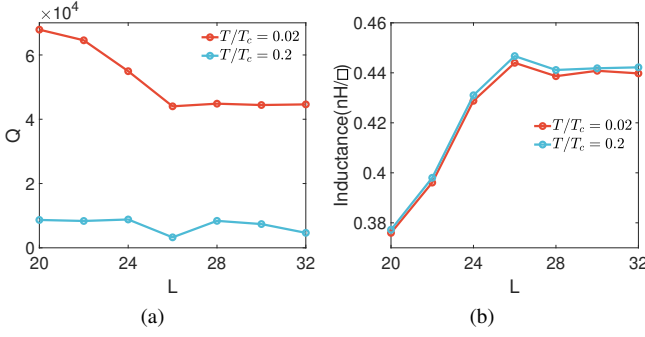


Figure 1. The quality factor  $Q$  (a) and the kinetic inductance  $L_k/\square$  (b) as a function of system size  $L$  for  $U = -1$ ,  $\langle n \rangle = 0.875$ ,  $f = 0.028\Delta_0$ , and  $V = 1.5$ , close to the critical disorder, which is the main focus of the paper. No substantial size dependence is observed for  $L \geq 26$ , so we fix the size  $L = 28$  in our study. For stronger disorder or coupling, finite size effects will be even smaller.

$\frac{f}{\Delta f}$ , where  $f$  is the circuit operating frequency (measured in Hertz).  $Q$  describes the frequency resolution  $\Delta f$  which is closely related to the strength of dissipative effects leading to electromagnetic absorption and therefore to circuit losses. The total quality factor of the circuit has two components,  $\frac{1}{Q} = \frac{1}{Q_i} + \frac{1}{Q_{ext}}$  [60] where  $Q_i$  is the internal quality factor computed in the paper due to losses in the superinductor, and  $Q_{ext}$  is the external quality factor related to any other losses.  $Q_{ext}$  is typically much higher than  $Q_i$  in the experimental settings that we are interested in, so  $Q \approx Q_i$ .

Two superinductor geometries are especially relevant for applications: superconducting micro-strips lines for quantum computing and cavity resonators for phonon detection. We shall see that the main findings of the paper are applicable to both settings though  $Q$  in each case is different by an overall disorder and temperature independent prefactor. From now on, we focus on the micro-strip setup, the cavity resonator is discussed in the Supplemental information [61]. The quality factor of the micro-strip is [62–64]  $Q = \frac{\alpha}{2\beta}$ , where  $\alpha$  and  $\beta$  are the real and imaginary parts of the propagation constant  $\gamma$ . For dissipative media, [62, 64]  $\gamma = \sqrt{i\omega\mu(\sigma + i\omega\epsilon)} = \alpha + i\beta$ , where  $\epsilon$  and  $\mu$  are the permittivity and permeability of the media, and  $\sigma = \sigma_1 - i\sigma_2$ , where  $\sigma_1$  and  $\sigma_2$  are the real and imaginary parts of the conductivity  $\sigma$ . Since  $\sigma_2 \gg \sigma_1$ , and the device operates at microwave frequencies [62, 63],  $Q \approx \sigma_2/\sigma_1$ . Likewise, the kinetic inductance is  $L_k/\square = \frac{1}{2\pi f\sigma_2}$ .

*Theoretical formalism.*— In order to compute  $L_k/\square$  and  $Q$ , we model the resonator as a disordered superconducting thin film with  $N = L \times L$  sites described by the BdG equations [57, 58, 65, 66],

$$\begin{pmatrix} \hat{K} & \hat{\Delta} \\ \hat{\Delta}^* & -\hat{K}^* \end{pmatrix} \begin{pmatrix} u_m(i) \\ v_m(i) \end{pmatrix} = E_m \begin{pmatrix} u_m(i) \\ v_m(i) \end{pmatrix} \quad (1)$$

where  $\hat{K}u_m(i) = -t\sum_{\delta} u_m(i + \delta) + (V_i - \mu_i)u_m(i)$ ,  $V_i$

is a random potential  $V_i \in [-V, V]$ ,  $\mu_i = \mu + |U|n(i)/2$  is the chemical potential that incorporates the site-dependent Hartree shift,  $U$  is the net attractive electronic coupling, and  $\delta$  is restricted to nearest neighbors of site  $i$ . The BdG equations are completed by the self-consistent conditions for the site-dependent order parameter amplitude  $\Delta(i) = |U|\sum_m u_m(i)v_m^*(i)(1 - 2f(E_m, T))$  and the density  $n(i) = 2\sum_m [|v_m(i)|^2(1 - f(E_m, T)) + |u_m(i)|^2f(E_m, T)]$  where  $f(E_m, T) = \frac{1}{e^{E_m/T} + 1}$  is the Fermi-Dirac distribution at temperature  $T$ . The average electron density is  $\langle n \rangle = \sum_i n(i)/N = 0.875$  with  $N$  the total number of sites of the square lattice. This choice, previously used in [29, 65–67], leads to [68] suppression of charge-density wave correlations while keeping the order parameter as large as possible. All these quantities are in units of the hopping energy  $t$ . Based on the solutions of these equations, we compute current-current correlation functions beyond the mean-field BdG limit within a gauge invariant random phase approximation which amounts to considering vertex corrections to the bare bubble diagrams representing the susceptibility. Finally, we compute the complex conductivity from which, as mentioned earlier, is straightforward to find  $Q(T, V, U)$  and  $L_k/\square(T, V, U)$  [see Supplemental information [61] for technical details]. Our study is focused on the metallic side of the superconductor-insulator transition where we will also compute the distribution of probability of  $Q$  to assess the role of multifractality and to have an estimate of sample to sample fluctuations which are important in experiments. The choice of parameters in our calculation is motivated by the following considerations: a superconductor resonator typically works in the microwave region 1 – 20 GHz [2, 7, 10, 69–72], which in units of energy corresponds to  $4.0 \times 10^{-3} - 8.0 \times 10^{-2}$  meV. Therefore, we set the hopping energy to  $t = 10$  meV so that the operating frequencies of the device lie in the range 1 – 20 GHz. We will focus on two typical frequencies  $f \sim 0.001t = 0.028\Delta_0$  and  $0.004t = 0.112\Delta_0$  corresponding to 2.5 GHz and 10 GHz respectively. The lattice constant is set to  $a = 0.35$  nm and the permittivity  $\epsilon = 9\epsilon_0$ . We note that all the calculation is carried in SI units, which can compare with experiments directly. In order to have a larger  $Q$ , temperatures must be much lower than the critical one i.e.  $T \ll T_c$ , but still accessible experimentally  $T \sim 0.01 - 0.15T_c$ . We model weakly coupled superconductors by a coupling constant  $U = -1$ , in units of  $t$ , because this is the smallest coupling for which the finite size effects in our calculation are negligible. For these parameters, we obtain for  $V = 0$  an order parameter  $\Delta_0 = 0.0357t = 0.357$  meV and a critical temperature  $T_c \sim 0.02t \sim 2.3$  K.

*Finite-size effects.*— We start our analysis of  $L_k/\square$  and  $Q$  by showing that finite size effects are not important. In Fig. 1, we depict  $Q$  for different system sizes  $L$  and for two different temperatures. We do not observe any substantial size dependence for  $L \geq 26$ . Finite size effects in  $Q$  are much stronger for small sizes because quantum fluctuations increase as the system size decreases. Finite temperature effects, as observed

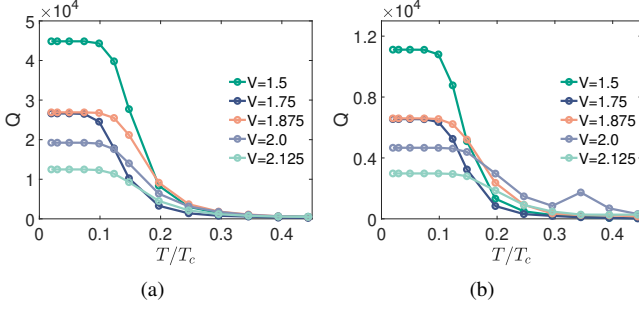


Figure 2. Quality factor  $Q$  as a function of temperature for a lattice of size  $L = 28$  and different disorder strengths  $V$ ,  $U = -1$  and  $\langle n \rangle = 0.875$ .  $Q$  is computed using 70 disorder realization for each  $V$ , except for  $V = 2.125$  where we employ only 20. The frequency is, (a)  $f = 0.028\Delta_0 \sim 2.5$  GHz (b)  $f = 0.112\Delta_0 \sim 10$  GHz.

in Fig. 1 suppress quantum fluctuations. The increase (decrease) of  $L_k/\square$  ( $Q$ ) with system size is due to the fact that  $L_k/\square$  is inversely proportional to  $\sigma_2$  while  $Q$  is directly proportional to it. For a stronger coupling constant  $|U| > 1$ , finite size effects are smaller because the coherence length is shorter. Therefore, from now on we set  $L = 28$ .

*Temperature, disorder and frequency dependence of the Quality factor.*— At sufficiently high temperatures,  $Q$  decreases sharply due to the increasing number of thermal quasiparticles [71]. Therefore, this region is not of interest in our analysis. In the superconducting region,  $\frac{1}{Q}$  is proportional to the remaining number of thermal quasiparticles, which will be reduced greatly by decreasing temperature [10, 71]. As a consequence,  $Q$  will increase substantially with decreasing temperature. However, as Fig. 2 shows, this increase levels off for sufficiently low  $T \leq 0.1T_c$  which is roughly consistent with experimental results [72]. The origin of this saturation of  $Q$  is due to quantum fluctuations [30, 32], captured in our analysis by the employed gauge-invariant random phase approximation, that smear out the real conductivity so that it is finite even below the spectral gap. Since  $Q$  is a decreasing function of temperature, the optimal operation of the device will always occur at the lowest temperature that can be reached experimentally though large values of  $Q$  can still be observed for  $T \sim 0.1T_c$ . We note that we are assuming a thermal distribution of quasiparticles but there is substantial evidence that in the low temperature limit, the distribution may be non-thermal [73, 74]. However, the quality factor measured experimentally [63] is still quite large  $Q > 10^4$ , so we do not expect that our main results are altered qualitatively by considering a non-thermal distribution.

Regarding the dependence on disorder, for sufficiently low temperatures,  $Q$  decreases sharply as disorder is increased, see Fig. 2. This is expected as both quantum fluctuations and spatial inhomogeneities facilitate the absorption of the incoming electromagnetic radiation and therefore the decrease of  $Q$ . Despite of this decrease,  $Q$  is still large  $\sim 10^4$  for  $f \sim 2.5$

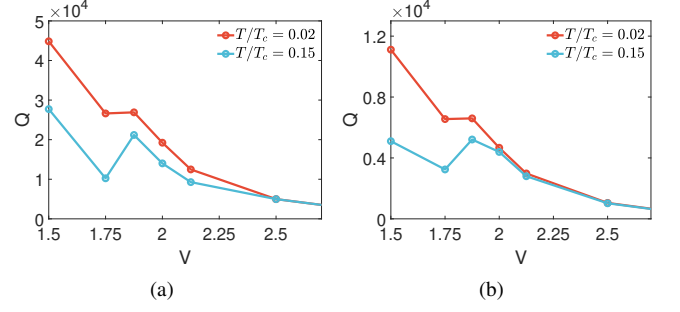


Figure 3. The quality factor  $Q$  as a function of disorder  $V$  for  $T/T_c = 0.02$  and  $0.15$  at the experimental frequencies (a)  $f \sim 2.5$  GHz and (b)  $f \sim 10$  GHz.  $Q$  increases with disorder in the critical region close to the transition,  $V \simeq 1.9$ . This non-monotonicity of  $Q$  occurs for others  $T \gtrsim 0.1T_c$  and  $f$ , but only for  $V \simeq 1.9$ . See Fig. 2 for the value of the rest of parameters.

GHz and  $\sim 5 \times 10^3$  for  $f \sim 10$  GHz, in the sub-gap frequency region of interest provided that the disorder strength is not too strong  $V \lesssim 2$  where  $V$  is expressed in units of  $t$ . The  $V > 2$  insulating region is of no interest for applications. The disorder dependence of  $Q$ , for small but finite  $T \gtrsim 0.1T_c$ , shows an unexpected non-monotonous behavior in the critical region  $V \sim 1.9$ , see Fig. 2. In order to fully confirm it, in Fig. 3, we depict  $Q$  in linear scale as a function of  $V$ . The non-monotonicity is clearly observed in a relatively small window of temperatures, and only in the critical region  $V \simeq 1.9$ , but its effect is rather strong. Below, we provide a tentative explanation of this property which is one of the main results of the paper. The dependence of  $Q$  on frequency is monotonous, it decreases rapidly with increasing frequency. The optimal setting is therefore the smallest frequency that can be accessible to experiments [61].

*Kinetic inductance.*— We now turn to the study of  $L_k/\square$ . The analysis is simpler because it grows monotonically with  $V$  and it is weakly dependent on frequency for frequencies below the so called two-particle gap, namely, the frequency required to break a Cooper pair [75]. Since the resistance increases exponentially with disorder, we expect a similar behavior in the kinetic inductance  $L_k/\square$ . In qualitative agreement with the experimental results [6–8, 14, 76], see Fig. 4, disorder enhances  $L_k/\square$  by up to two orders of magnitude in the metallic region  $V \lesssim 2$  where our formalism is applicable.

*Critical disorder and optimal choice of parameters.*— Since  $L_k/\square$  increases sharply with disorder, and a large  $Q$  requires  $V \leq 2$ , it is important to have an estimation of the critical disorder strength  $V_c$  at which the insulating transition takes place. The result of an approximate percolation analysis suggests  $V_c \sim 2$ . This is consistent with an earlier [37] estimate  $V_c \sim 1.5$  in a similar system based on level statistics and the vanishing of the superfluid density. At this  $V$ , the spectral gap also starts to increase with disorder which is another indication [65, 66] of the transition [see Supplemental information

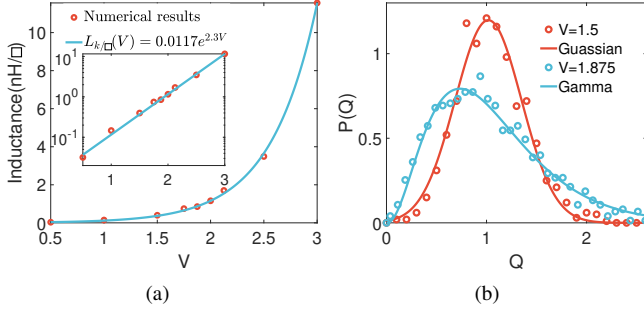


Figure 4. Left: The kinetic inductance  $L_{k/\square}$  as a function of disorder  $V$ . The other parameters are the same as those in Fig. 2. The numerical results fit well with an exponential increase of  $L_{k/\square}$  with disorder. In the Supplemental Material [61] we show that in the region of interest  $f \in [2.5, 10]$  GHz,  $T \ll T_c$ ,  $L_{k/\square}$  is almost temperature and frequency independent. Right: Probability distribution of  $Q$  from 1000 disorder realizations, normalized by its sample averaged value for  $f \sim 2.5$  GHz, and temperature  $T/T_c = 0.05$ . When  $V = 1.5$ , the distribution of  $Q$  fits well with a Gaussian distribution, red line. However, very close to the transition  $V \approx 1.9 \approx V_c$ , the distribution, asymmetric and with broad tails, is similar to a Gamma distribution (blue line).

[61] for more information].

Therefore, based also on the previous results,  $V \lesssim 1.9$ , corresponding to the strongest disorder still on the metallic side of the transition, is the optimal setting to observe an enhancement of  $L_{k/\square}$  without a large decrease in  $Q \geq 10^4$ . Regarding the rest of parameters, based on the previous analysis, the optimal conditions for operation of the superinductor are weak-coupling  $|U| \leq 1$ , frequencies  $f \sim 2.5 - 10$  GHz well below the two-particle spectral gap and the lowest accessible temperature. However,  $T \gtrsim 0.15T_c \ll T_c$  is still close to this optimal value and we could also observe in  $Q$  an intriguing non-monotonous dependence on disorder.

With these choices,  $L_{k/\square}$  increases up to two orders of magnitude with  $V$ , and this is not accompanied by strong dissipation since  $Q \gtrsim 10^4$  even for  $V \lesssim 1.9$ . In order to describe quantitatively the experimental results, it would be necessary to have a precise relation between  $V$  and the experimental resistivity  $\rho_{dc}$  which is a difficult task. We can only say that the region  $V \sim 1.9$  of main interest corresponds experimentally to the metallic side of the transition. Perturbatively,  $\rho_{dc} \propto \langle V^2 \rangle$  for a non-interacting disordered metal [67].

**Discussion and conclusions.**— Previously, we found that close to the transition  $V_c \simeq 1.9$ , and for  $T \gtrsim 0.1T_c$ , disorder can even enhance the quality factor. We first address the origin of this counter-intuitive feature. In principle, by increasing disorder, the order parameter is weakened in parts of the sample which become optically active more easily and lead to the decrease of  $Q$ . However, the order parameter spatial distribution close to the transition has multifractal-like features [37, 38] like a broad log-normal probability distribution [77] which

adds a twist to this argument. At zero or low temperature  $T \ll T_c$ , metallic regions with a large value of the order parameter amplitude coexist with regions where it is close to zero or with incipient Anderson localization effects.

By a slight increase in disorder, it is plausible that regions with a large value of the order parameter remain largely unaltered while the rest may effectively become an Anderson insulator. Unlike metallic but not superconducting regions, those insulating regions do not absorb the incoming electromagnetic radiation. Its net effect is a reduction of optically active regions and therefore an increase of  $Q$  with disorder.

As a consequence, the observed sharp drop of  $Q$  with temperature occurs at higher temperatures, see Fig. 2(a), and there exists a relatively narrow region of temperatures  $T \sim 0.15T_c$ , for  $V \approx V_c$ , where the  $V$  dependence on  $Q$  is non-monotonic, namely,  $Q$  increases with disorder for  $V \sim V_c$ .

The qualitative changes of  $Q$  close to the transition  $V_c \simeq 1.9$  (see Fig. 4) are illustrated by computing the probability distribution obtained from 1000 disorder realizations. Even for  $V = 1.5$ , the distribution is close to a Gaussian. However, for  $V_c \approx 1.9$ , it becomes broad and asymmetric signaling large sample to sample fluctuations. This is the region where the order parameter spatial distribution has multifractal-like features so we believe that the anomalous enhancement of  $Q$  is related to this feature. We stress that the employed theoretical formalism is gauge invariant and therefore it is capable to account for collective excitations [26, 78] that lower dramatically the quality factor of the device. We have found [33] that indeed collective excitations may occur in weakly-coupled disordered superconductors. However, it is necessary to have a disorder larger than  $V_c \simeq 1.9$  for the collective excitations to be observed for the frequencies  $2.5 - 10$  GHz of interest. Therefore, collective excitations do not seem to play any role in the superinductor optimal region of operation.

The coupling we employ  $U = -1$  and  $\langle n \rangle = 0.875$  is too strong to describe granular Al [14] experiments. However, we expect similar [79] physics is at play though the interplay of collective modes and granularity require a separate study. Note that we neglect Coulomb interactions. It has been recently argued [14, 80] that Coulomb interactions may play an important role in granular Al close to the insulating transition. However, on the metallic region of interest, charging effects are screened and therefore do not play an important role.

In conclusion, we have found that strongly-disordered, weakly-coupled superconducting thin films are excellent superinductors with  $L_{k/\square}$  enhanced up to two orders of magnitude by disorder while  $Q \gtrsim 10^4$ . Moreover, close to the superconductor-insulator transition  $Q$  has a broad probability distribution and, counterintuitively, is enhanced by disorder. Despite the limitations mentioned previously, the enhancement of  $L_{k/\square}$  with disorder and the mild decrease, and even enhancement in some cases, of  $Q$  with disorder, are robust, can be confirmed experimentally and be used to improve the superinductor performance.

B.F. and A.M.G.G. acknowledge financial support from a Shanghai talent program, from the National Natural Sci-



ence Foundation China (NSFC) (Grant No. 11874259) and from the National Key R&D Program of China (Project ID: 2019YFA0308603). A.S. acknowledges the computational facilities of Physics Department, Technion.

\* [bo.fan@sjtu.edu.cn](mailto:bo.fan@sjtu.edu.cn)

† [abhiseks@campus.technion.ac.il](mailto:abhiseks@campus.technion.ac.il)

‡ [amgg@sjtu.edu.cn](mailto:amgg@sjtu.edu.cn)

- [1] J. Q. You, J. S. Tsai, and Franco Nori. Scalable quantum computing with josephson charge qubits. *Phys. Rev. Lett.*, 89:197902, Oct 2002.
- [2] Xiu Gu, Anton Frisk Kockum, Adam Miranowicz, Yu-xi Liu, and Franco Nori. Microwave photonics with superconducting quantum circuits. *Physics Reports*, 718:1–102, 2017.
- [3] Morten Kjaergaard, Mollie E Schwartz, Jochen Braumüller, Philip Krantz, Joel I-J Wang, Simon Gustavsson, and William D Oliver. Superconducting qubits: Current state of play. *Annual Review of Condensed Matter Physics*, 11:369–395, 2020.
- [4] J. T. Peltonen, O. V. Astafiev, Yu. P. Korneeva, B. M. Voronov, A. A. Korneev, I. M. Charaev, A. V. Semenov, G. N. Golt’sman, L. B. Ioffe, T. M. Klapwijk, and J. S. Tsai. Coherent flux tunneling through nbn nanowires. *Phys. Rev. B*, 88:220506, Dec 2013.
- [5] Vladimir E. Manucharyan, Jens Koch, Leonid I. Glazman, and Michel H. Devoret. Fluxonium: Single cooper-pair circuit free of charge offsets. *Science*, 326(5949):113–116, 2009.
- [6] Anthony J Annunziata, Daniel F Santavica, Luigi Frunzio, Gianluigi Catelani, Michael J Rooks, Aviad Frydman, and Daniel E Prober. Tunable superconducting nanoinductors. *Nanotechnology*, 21(44):445202, oct 2010.
- [7] David Niepce, Jonathan Burnett, and Jonas Bylander. High kinetic inductance NbN nanowire superinductors. *Phys. Rev. Applied*, 11:044014, Apr 2019.
- [8] Wenyuan Zhang, K. Kalashnikov, Wen-Sen Lu, P. Kamenov, T. DiNapoli, and M.E. Gershenson. Microresonators fabricated from high-kinetic-inductance aluminum films. *Phys. Rev. Applied*, 11:011003, Jan 2019.
- [9] H Rotzinger, S T Skacel, M Pfirrmann, J N Voss, J Münzberg, S Probst, P Bushev, M P Weides, A V Ustinov, and J E Mooij. Aluminium-oxide wires for superconducting high kinetic inductance circuits. *Superconductor Science and Technology*, 30(2):025002, nov 2017.
- [10] Francesco Valenti, Fabio Henriques, Gianluigi Catelani, Nataliya Maleeva, Lukas Grunhaupt, Uwe von Lupke, Sebastian T. Skacel, Patrick Winkel, Alexander Bilmes, Alexey V. Ustinov, Johannes Goupy, Martino Calvo, Alain Benoît, Florence Levy-Bertrand, Alessandro Monfardini, and Ioan M. Pop. Interplay between kinetic inductance, nonlinearity, and quasiparticle dynamics in granular aluminum microwave kinetic inductance detectors. *Phys. Rev. Applied*, 11:054087, May 2019.
- [11] Lukas Grünhaupt, Nataliya Maleeva, Sebastian T. Skacel, Martino Calvo, Florence Levy-Bertrand, Alexey V. Ustinov, Hannes Rotzinger, Alessandro Monfardini, Gianluigi Catelani, and Ioan M. Pop. Loss mechanisms and quasiparticle dynamics in superconducting microwave resonators made of thin-film granular aluminum. *Phys. Rev. Lett.*, 121:117001, Sep 2018.
- [12] N. Maleeva, L. Grünhaupt, T. Klein, F. Levy-Bertrand, O. Dupre, M. Calvo, F. Valenti, P. Winkel, F. Friedrich, W. Wernsdorfer, and et al. Circuit quantum electrodynamics of granular aluminum resonators. *Nature Communications*, 9(1), Sep 2018.
- [13] Lukas Grunhaupt, Martin Spiecker, Daria Gusenkova, Nataliya Maleeva, Sebastian T. Skacel, Ivan Takmakov, Francesco Valenti, Patrick Winkel, Hannes Rotzinger, Wolfgang Wernsdorfer, and et al. Granular aluminium as a superconducting material for high-impedance quantum circuits. *Nature Materials*, 18(8):816–819, Apr 2019.
- [14] Aviv Glezer Moshe, Eli Farber, and Guy Deutscher. Granular superconductors for high kinetic inductance and low loss quantum devices. *Applied Physics Letters*, 117(6):062601, Aug 2020.
- [15] Patrick Winkel, Kiril Borisov, Lukas Grünhaupt, Dennis Rieger, Martin Spiecker, Francesco Valenti, Alexey V. Ustinov, Wolfgang Wernsdorfer, and Ioan M. Pop. Implementation of a transmon qubit using superconducting granular aluminum. *Phys. Rev. X*, 10:031032, Aug 2020.
- [16] Fang Yang, Thomas Gozliniski, Tim Storbeck, Lukas Grünhaupt, Ioan M. Pop, and Wulf Wulfhelke. Microscopic charging and in-gap states in superconducting granular aluminum. *Phys. Rev. B*, 102:104502, Sep 2020.
- [17] O Dupré, A Benoît, M Calvo, A Catalano, J Goupy, C Hoarau, T Klein, K Le Calvez, B Sacépé, A Monfardini, and et al. Tunable sub-gap radiation detection with superconducting resonators. *Superconductor Science and Technology*, 30(4):045007, Feb 2017.
- [18] SE De Graaf, ST Skacel, T Hönlgl-Decrinis, R Shaikhaidarov, H Rotzinger, S Linzen, M Ziegler, U Hübner, H-G Meyer, V Antonov, et al. Charge quantum interference device. *Nature Physics*, 14(6):590–594, 2018.
- [19] P. C. J. J. Coumou, E. F. C. Driessen, J. Bueno, C. Chapelier, and T. M. Klapwijk. Electrodynamic response and local tunneling spectroscopy of strongly disordered superconducting tin films. *Phys. Rev. B*, 88:180505, Nov 2013.
- [20] G. Deutscher, H. Fenichel, M. Gershenson, E. Grünbaum, and Z. Ovadyahu. Transition to zero dimensionality in granular aluminum superconducting films. *J. Low Temp. Phys.*, 10(1-2):231–243, January 1973.
- [21] G. Deutscher, M. Gershenson, E. Grünbaum, and Y. Imry. Granular Superconducting Films. *J. Vac. Sci. Technol.*, 10(5):697, September 1973.
- [22] B Abeles. Effect of charging energy on superconductivity in granular metal films. *Phys. Rev. B*, 15(5):2828, 1977.
- [23] B. Abeles, Roger W. Cohen, and G. W. Cullen. Enhancement of Superconductivity in Metal Films. *Phys. Rev. Lett.*, 17(12):632–634, September 1966.
- [24] Robert Meservey and Paul M Tedrow. Measurements of the kinetic inductance of superconducting linear structures. *Journal of Applied Physics*, 40(5):2028–2034, 1969.
- [25] P. W. Anderson. Random-phase approximation in the theory of superconductivity. *Phys. Rev.*, 112:1900–1916, Dec 1958.
- [26] P. W. Anderson. Plasmons, gauge invariance, and mass. *Phys. Rev.*, 130:439–442, Apr 1963.
- [27] D. C. Mattis and J. Bardeen. Theory of the anomalous skin effect in normal and superconducting metals. *Phys. Rev.*, 111:412–417, Jul 1958.
- [28] Jeffrey Goldstone. Field theories with «superconductor» solutions. *Il Nuovo Cimento (1955-1965)*, 19(1):154–164, 1961.
- [29] G. Seibold, L. Benfatto, and C. Castellani. Application of the mattis-bardeen theory in strongly disordered superconductors. *Phys. Rev. B*, 96:144507, Oct 2017.
- [30] T. Cea, D. Bucheli, G. Seibold, L. Benfatto, J. Lorenzana, and C. Castellani. Optical excitation of phase modes in strongly disordered superconductors. *Phys. Rev. B*, 89:174506, May 2014.
- [31] T. Cea, C. Castellani, G. Seibold, and L. Benfatto. Nonrelativis-

- tic dynamics of the amplitude (higgs) mode in superconductors. *Phys. Rev. Lett.*, 115:157002, Oct 2015.
- [32] Abhisek Samanta, Amulya Ratnakar, Nandini Trivedi, and Rajdeep Sensarma. Two-particle spectral function for disordered *s*-wave superconductors: Local maps and collective modes. *Phys. Rev. B*, 101:024507, Jan 2020.
- [33] Bo Fan, Abhisek Samanta, and Antonio M. García-García. Characterization of collective excitations in weakly coupled disordered superconductors. *Phys. Rev. B*, 105:094515, Mar 2022.
- [34] John M. Martinis, K. B. Cooper, R. McDermott, Matthias Steffen, Markus Ansmann, K. D. Osborn, K. Cicak, Seongshik Oh, D. P. Pappas, R. W. Simmonds, and Clare C. Yu. Decoherence in josephson qubits from dielectric loss. *Phys. Rev. Lett.*, 95:210503, Nov 2005.
- [35] Jiansong Gao. The physics of superconducting microwave resonators. dissertation (ph.d.), california institute of technology, 2008.
- [36] James Mayoh and Antonio M. García-García. Global critical temperature in disordered superconductors with weak multifractality. *Phys. Rev. B*, 92:174526, Nov 2015.
- [37] Bo Fan and Antonio M. García-García. Enhanced phase-coherent multifractal two-dimensional superconductivity. *Phys. Rev. B*, 101:104509, Mar 2020.
- [38] Bo Fan and Antonio M. García-García. Superconductivity at the three-dimensional anderson metal-insulator transition. *Phys. Rev. B*, 102:184507, Nov 2020.
- [39] I. S. Burmistrov, I. V. Gornyi, and A. D. Mirlin. Enhancement of the Critical Temperature of Superconductors by Anderson Localization. *Phys. Rev. Lett.*, 108(1):017002, January 2012.
- [40] James Mayoh and Antonio M. García-García. Number theory, periodic orbits, and superconductivity in nanocubes. *Phys. Rev. B*, 90(1):014509, July 2014.
- [41] J. Mayoh and A. M. García-García. Strong enhancement of bulk superconductivity by engineered nanogranularity. *Phys. Rev. B*, 90(13):134513, October 2014.
- [42] I. S. Burmistrov, I. V. Gornyi, and A. D. Mirlin. Superconductor-insulator transitions: Phase diagram and magnetoresistance. *Phys. Rev. B*, 92:014506, Jul 2015.
- [43] Masaki Tezuka and Antonio M. García-García. Stability of the superfluid state in a disordered one-dimensional ultracold fermionic gas. *Physical Review A*, 82(4), Oct 2010.
- [44] M. V. Feigel'man, L. B. Ioffe, V. E. Kravtsov, and E. A. Yuzbashyan. Eigenfunction fractality and pseudogap state near the superconductor-insulator transition. *Phys. Rev. Lett.*, 98:027001, Jan 2007.
- [45] R.H. Parmenter. Size Effect in a Granular Superconductor. *Phys. Rev.*, 166(2):392–396, February 1968.
- [46] A. A. Shanenko, M. D. Croitoru, and F. M. Peeters. Oscillations of the superconducting temperature induced by quantum well states in thin metallic films: Numerical solution of the Bogoliubov-de Gennes equations. *Phys. Rev. B*, 75(1):014519, January 2007.
- [47] Antonio M García-García, Juan Diego Urbina, Emil A Yuzbashyan, Klaus Richter, and Boris L Altshuler. Bardeen-cooper-schrieffer theory of finite-size superconducting metallic grains. *Physical review letters*, 100(18):187001, 2008.
- [48] Antonio M. García-García, Juan D Urbina, Emil A. Yuzbashyan, Klaus Richter, and Boris L. Altshuler. BCS superconductivity in metallic nanograins: Finite-size corrections, low-energy excitations, and robustness of shell effects. *Phys. Rev. B*, 83(1):014510, January 2011.
- [49] C. Brun, T. Cren, V. Cherkez, F. Debontridder, S. Pons, D. Fokin, M. C. Tringides, S. Bozhko, L. B. Ioffe, B. L. Altshuler, et al. Remarkable effects of disorder on superconductivity of single atomic layers of lead on silicon. *Nature Physics*, 10:444–450, April 2014.
- [50] Kun Zhao, Haicheng Lin, Xiao Xiao, Wantong Huang, Wei Yao, Mingzhe Yan, Ying Xing, Qinghua Zhang, Zi-Xiang Li, Shintaro Hoshino, et al. Disorder induced multifractal superconductivity in monolayer niobium dichalcogenides. *arXiv preprint arXiv:1904.07076 Nat. Phys.* 15, 904, 2019.
- [51] Carmen Rubio-Verdu, Antonio M. García-García, Hyejin Ryu, Deung-Jang Choi, Javier Zaldivar, Shujie Tang, Bo Fan, Zhi-Xun Shen, Sung-Kwan Mo, Jose Ignacio Pascual, and Miguel M. Ugeda. Visualization of multifractal superconductivity in a two-dimensional transition metal dichalcogenide in the weak-disorder regime. *Nano Letters*, 20(7):5111–5118, 2020.
- [52] Uwe S. Pracht, Nimrod Bachar, Lara Benfatto, Guy Deutscher, Eli Farber, Martin Dressel, and Marc Scheffler. Enhanced cooper pairing versus suppressed phase coherence shaping the superconducting dome in coupled aluminum nanograins. *Phys. Rev. B*, 93:100503, Mar 2016.
- [53] Uwe S. Pracht, Tommaso Cea, Nimrod Bachar, Guy Deutscher, Eli Farber, Martin Dressel, Marc Scheffler, Claudio Castellani, Antonio M. García-García, and Lara Benfatto. Optical signatures of the superconducting goldstone mode in granular aluminum: Experiments and theory. *Phys. Rev. B*, 96:094514, Sep 2017.
- [54] Sangita Bose, Antonio M. García-García, Miguel M. Ugeda, Juan D. Urbina, Christian H. Michaelis, Ivan Brihuega, and Klaus Kern. Observation of shell effects in superconducting nanoparticles of Sn. *Nat. Mater.*, 9(7):550–554, July 2010.
- [55] Zhi Li, Jun-Ping Peng, Hui-Min Zhang, Can-Li Song, Shuai-Hua Ji, Lili Wang, Ke He, Xi Chen, Qi-Kun Xue, and Xu-Cun Ma. Visualizing superconductivity in fese nanoflakes on srtio<sub>3</sub> by scanning tunneling microscopy. *Phys. Rev. B*, 91:060509, Feb 2015.
- [56] Ivan Brihuega, Pedro Ribeiro, Antonio M. Garcia-Garcia, Miguel M. Ugeda, Christian H. Michaelis, Sangita Bose, Klaus Kern, and Antonio García-García. Experimental observation of thermal fluctuations in single superconducting Pb nanoparticles through tunneling measurements. *Phys. Rev. B*, 84(10):104525, April 2011.
- [57] P.G. de Gennes. Boundary Effects in Superconductors. *Rev. Mod. Phys.*, 36(1):225–237, January 1964.
- [58] P.G. de Gennes. *Superconductivity of Metals and Alloys*. W.A. Bebjamin, inc., New York, 1966.
- [59] M. V. Feigel'man and L. B. Ioffe. Microwave properties of superconductors close to the superconductor-insulator transition. *Phys. Rev. Lett.*, 120:037004, Jan 2018.
- [60] Daniel Hafner, Martin Dressel, and Marc Scheffler. Surface-resistance measurements using superconducting stripline resonators. *Review of Scientific Instruments*, 85(1):014702, 2014.
- [61] See supplemental material at <http://link.aps.org/supplemental/10.1103/PhysRevLett.130.047001> for discussions about: (i) the theoretical model and the technical details related to the calculation of quality factor and kinetic inductance in disordered superconductors, (ii) temperature dependence of the sample-averaged quality factor and kinetic inductance for different disorder strengths, (iii) the quality factor for a cavity, and (iv) the estimation of critical disorder using the spectral gap and a percolation analysis.
- [62] Ghassan Yassin and S Withington. Electromagnetic models for superconducting millimetre-wave and sub-millimetre-wave microstrip transmission lines. *Journal of Physics D: Applied Physics*, 28(9):1983, 1995.

- [63] P. J. de Visser, D. J. Goldie, P. Diener, S. Withington, J. J. A. Baselmans, and T. M. Klapwijk. Evidence of a nonequilibrium distribution of quasiparticles in the microwave response of a superconducting aluminum resonator. *Phys. Rev. Lett.*, 112:047004, Jan 2014.
- [64] David Keun Cheng et al. *Field and wave electromagnetics*. Pearson Education India, 1989.
- [65] Amit Ghosal, Mohit Randeria, and Nandini Trivedi. Inhomogeneous pairing in highly disordered s-wave superconductors. *Phys. Rev. B*, 65(1):014501, November 2001.
- [66] Amit Ghosal, Mohit Randeria, and Nandini Trivedi. Role of spatial amplitude fluctuations in highly disordered s-wave superconductors. *Phys. Rev. Lett.*, 81:3940–3943, Nov 1998.
- [67] Anushree Datta, Anurag Banerjee, Nandini Trivedi, and Amit Ghosal. New paradigm for a disordered superconductor in a magnetic field. 2021.
- [68] Carey Huscroft and Richard T. Scalettar. Evolution of the density of states gap in a disordered superconductor. *Phys. Rev. Lett.*, 81:2775–2778, Sep 1998.
- [69] Lukas Grünhaupt, Martin Spiecker, Daria Gusenkova, Nataliya Maleeva, Sebastian T Skacel, Ivan Takmakov, Francesco Valenti, Patrick Winkel, Hannes Rotzinger, Wolfgang Wernsdorfer, et al. Granular aluminium as a superconducting material for high-impedance quantum circuits. *Nature materials*, 18(8):816–819, 2019.
- [70] Philip Krantz, Morten Kjaergaard, Fei Yan, Terry P Orlando, Simon Gustavsson, and William D Oliver. A quantum engineer’s guide to superconducting qubits. *Applied Physics Reviews*, 6(2):021318, 2019.
- [71] AV Sergeev, VV Mitin, and BS Karasik. Ultrasensitive hot-electron kinetic-inductance detectors operating well below the superconducting transition. *Applied physics letters*, 80(5):817–819, 2002.
- [72] Nodar Samkharadze, A Bruno, Pasquale Scarlino, G Zheng, DP DiVincenzo, L DiCarlo, and LMK Vandersypen. High-kinetic-inductance superconducting nanowire resonators for circuit qed in a magnetic field. *Physical Review Applied*, 5(4):044004, 2016.
- [73] Jhy-Jiun Chang and D. J. Scalapino. Kinetic-equation approach to nonequilibrium superconductivity. *Phys. Rev. B*, 15:2651–2670, Mar 1977.
- [74] R.E. Horstman and J. Wolter. Gap enhancement in narrow superconducting tunneljunctions induced by homogeneous microwave currents. *Physics Letters A*, 82(1):43–45, 1981.
- [75] Michael Tinkham. *Introduction to superconductivity*. Courier Corporation, 2004.
- [76] M. Peruzzo, A. Trioni, F. Hassani, M. Zemlicka, and J. M. Fink. Surpassing the resistance quantum with a geometric superinductor. *Phys. Rev. Applied*, 14:044055, Oct 2020.
- [77] James Mayoh and Antonio M. García-García. Global critical temperature in disordered superconductors with weak multifractality. *Phys. Rev. B*, 92:174526, Nov 2015.
- [78] Yoichiro Nambu. Quasi-particles and gauge invariance in the theory of superconductivity. *Phys. Rev.*, 117:648–663, Feb 1960.
- [79] JR Waldram. The josephson effects in weakly coupled superconductors. *Reports on Progress in Physics*, 39(8):751, 1976.
- [80] Aviv Glezer Moshe, Gal Tuvia, Shilo Avraham, Eli Farber, and Guy Deutscher. Tunneling study in granular aluminum near the mott metal-to-insulator transition. *Physical Review B*, 104(5), Aug 2021.
- [81] G. Seibold, L. Benfatto, C. Castellani, and J. Lorenzana. Amplitude, density, and current correlations of strongly disordered superconductors. *Phys. Rev. B*, 92:064512, Aug 2015.
- [82] Plamen Kamenov, Wen-Sen Lu, Konstantin Kalashnikov, Thomas DiNapoli, Matthew T Bell, and Michael E Gershenson. Granular aluminum meandered superinductors for quantum circuits. *Physical Review Applied*, 13(5):054051, 2020.
- [83] D Stauffer and A Aharony. *Introduction to percolation theory* (2003). London: Taylor & Francis, 2003.
- [84] P Dean and NF Bird. Monte carlo estimates of critical percolation probabilities. In *Mathematical Proceedings of the Cambridge Philosophical Society*, volume 63, pages 477–479. Cambridge University Press, 1967.

# Supplemental Material for “Tuning superinductors by quantum coherence effects for enhancing quantum computing”

In this supplemental information, we first introduce the theoretical model and present the technical and numerical details related to the calculation of the quality factor and the kinetic inductance at finite temperatures. Secondly, we show that around the critical disorder, finite size effects are not important in our analysis. Next, we present the temperature-dependent quality factor for a series of disorder strengths and frequencies by first computing the averaged conductivity. We also show that these results are similar to those obtained by computing the quality factor for each disorder realization and then performing ensemble average. The quality factor in the cavity case is also discussed for comparison. Finally, we make an estimation of the critical disorder at which the superconductor transition occurs by a percolation analysis and also by a study of the dependence of the spectroscopic gap with the disorder strength.

## CONTENTS

Calculation of the quality factor and the kinetic inductance from a gauge-invariant optical conductivity at finite temperature	8
Estimation of finite size effects	12
The Quality factor computed from the sample-averaged conductivity	13
The sample averaged Quality factor and Kinetic Inductance	14
The Quality factor for a cavity resonator	15
The estimation of critical disorder by percolation and the energy gap	16

## CALCULATION OF THE QUALITY FACTOR AND THE KINETIC INDUCTANCE FROM A GAUGE-INVARIANT OPTICAL CONDUCTIVITY AT FINITE TEMPERATURE

The microscopic Hamiltonian is an attractive Hubbard model on a square lattice in the presence of onsite disorder,

$$H = -t \sum_{\langle ij \rangle \sigma} c_{i\sigma}^\dagger c_{j\sigma} - U \sum_i n_{i\uparrow} n_{i\downarrow} + \sum_i V_i n_i \quad (S1)$$

where  $t$  is the nearest neighbor hopping energy and  $U$  is the attractive interaction between two electrons on the same site which leads to the Cooper pairing between them. The onsite random potential is drawn from a uniform distribution of zero mean and width  $2V$ , i.e.  $V_i \in [-V, V]$  where  $V$  is the strength of the disordered potential. Throughout the paper, we have used the values of  $U$  and  $V$  in units of  $t$ .

The goal of this section is to express the quality factor ( $Q$ ) and kinetic inductance ( $L_{k/\square}$ ), introduced in the main paper, in terms of the finite temperature conductivity, which includes vertex corrections to restore gauge invariance. Our starting point is the mean-field limit of this Hamiltonian, the so called BdG (Bogoliubov de-Gennes) Hamiltonian [57, 58], which depends on two parameters, the local superconducting order parameter  $\Delta(i)$  and the local density  $n(i)$  [65, 66]. We then invoke a canonical transformation (Bogoliubov transformation) to diagonalize the effective mean-field Hamiltonian. Note that since we are working in presence of random potential, the translational invariance of the system is broken and we need to diagonalize the large BdG Hamiltonian in real space. We obtain the eigenvalues  $E_n$  and eigenfunctions  $\{u_n(i), v_n(i)\}$ . With this information, we solve the self-consistent BdG mean-field equations iteratively on each site of the square lattice.

The next step is to use these mean-field results to study the optical response of the system at finite temperatures by an explicit calculation of the conductivity. This calculation includes corrections to the mean field results which are expressed in terms of the solutions of the BdG equation.

The conductivity depends on the following dynamical correlation function [29–31, 81],

$$\chi_{ij}(\phi, \phi') = -i \int dt e^{i\omega t} \langle [\phi_i(t), \phi'_j(0)] \rangle \quad (S2)$$



where  $\phi$  stands for the fluctuation components and the current operators given by [30]

$$\begin{aligned}
\delta\Delta_i &= c_{i\downarrow}c_{i\uparrow} - \langle c_{i\downarrow}c_{i\uparrow} \rangle \\
\delta\Delta_i^\dagger &= c_{i\uparrow}^\dagger c_{i\downarrow}^\dagger - \langle c_{i\uparrow}^\dagger c_{i\downarrow}^\dagger \rangle \\
\delta n_i &= \sum_\sigma \left( c_{i\sigma}^\dagger c_{i\sigma} - \langle c_{i\sigma}^\dagger c_{i\sigma} \rangle \right) \\
j_i^\alpha &= it \sum_\sigma \left( c_{i+\alpha,\sigma}^\dagger c_{i\sigma} - c_{i\sigma}^\dagger c_{i+\alpha,\sigma} \right).
\end{aligned} \tag{S3}$$

Here  $\delta\Delta_i$  is the fluctuation in the local superconducting order parameter around its mean-field value of  $\Delta(i)$ , and  $\delta n_i$  is the fluctuation in local density around its mean-field value of  $n(i)$ .  $\langle \dots \rangle$  denotes the expectation value of the operator in the inhomogeneous BdG eigenstate (obtained by diagonalizing the BdG matrix). The amplitude fluctuation  $A_i$  and the phase fluctuation  $\Phi_i$  of the superconducting order parameter  $\Delta(i)$  are therefore given by

$$A_i = (\delta\Delta_i + \delta\Delta_i^\dagger)/\sqrt{2} \tag{S4}$$

$$\Phi_i = i(\delta\Delta_i - \delta\Delta_i^\dagger)/\sqrt{2} \tag{S5}$$

Note that in our case, all the eigenvalues  $E_n$  and the corresponding eigenvectors  $\{u_n(i), v_n(i)\}$  of the BdG matrix are real. However here we present the formulas for different correlation functions at finite temperature  $T$  for the general case, where the eigenvectors are complex numbers.

The bare current-current correlation function [29–31, 81] is given by,

$$\begin{aligned}
\chi_{ij}(j^x, j^x) &= -2t^2 \sum_{nm} \frac{u_n^*(i+\hat{x})u_m(i)(u_m^*(j+\hat{x})u_n(j) - v_n(j+\hat{x})v_m^*(j))}{\omega + i\eta + E_n - E_m} (f(E_n) - f(E_m)) \\
&+ \frac{u_n^*(i+\hat{x})v_m^*(i)(v_m(j+\hat{x})u_n(j) + v_n(j+\hat{x})u_m(j))}{\omega + i\eta + E_n + E_m} (f(E_n) + f(E_m) - 1) \\
&+ \frac{v_n(i+\hat{x})u_m(i)(u_m^*(j+\hat{x})v_n^*(j) + u_n^*(j+\hat{x})v_m^*(j))}{\omega + i\eta - E_n - E_m} (1 - f(E_n) - f(E_m)) \\
&+ \frac{v_n(i+\hat{x})v_m^*(i)(u_n^*(j+\hat{x})u_m(j) - v_n(j+\hat{x})v_m^*(j))}{\omega + i\eta - E_n + E_m} (-f(E_n) + f(E_m)) \\
&- (j+\hat{x} \leftrightarrow j) - (i+\hat{x} \leftrightarrow i) + (i+\hat{x} \leftrightarrow i, j+\hat{x} \leftrightarrow j)
\end{aligned} \tag{S6}$$

where  $f(E_n) = \frac{1}{e^{E_n/T} + 1}$  is the Fermi-Dirac function. Similarly, the correlation function of the current operator  $j^x$  and the pair fluctuations  $(\delta\Delta, \delta\Delta^\dagger)$  or the charge fluctuations  $(\delta n)$  are given by,

$$\begin{aligned}
\chi_{ij}(j^x, \delta\Delta) &= 2it \sum_{nm} \frac{[u_n^*(i+\hat{x})u_m(i) - u_n^*(i)u_m(i+\hat{x})]u_n(j)v_m^*(j)}{\omega + i\eta + E_n - E_m} (f(E_n) - f(E_m)) \\
&- \frac{[u_n^*(i+\hat{x})v_m^*(i) - u_n^*(i)v_m^*(i+\hat{x})]u_m(j)u_n(j)}{\omega + i\eta + E_n + E_m} (f(E_n) + f(E_m) - 1) \\
&+ \frac{[v_n(i+\hat{x})u_m(i) - v_n(i)u_m(i+\hat{x})]v_m^*(j)v_n^*(j)}{\omega + i\eta - E_n - E_m} (1 - f(E_n) - f(E_m)) \\
&- \frac{[v_n(i+\hat{x})v_m^*(i) - v_n(i)v_m^*(i+\hat{x})]v_n^*(j)u_m(j)}{\omega + i\eta - E_n + E_m} (-f(E_n) + f(E_m))
\end{aligned} \tag{S7}$$

$$\begin{aligned}
\chi_{ij}(j^x, \delta\Delta^\dagger) &= 2it \sum_{nm} \frac{[u_n^*(i+\hat{x})u_m(i) - u_n^*(i)u_m(i+\hat{x})]u_m^*(j)v_n(j)}{\omega + i\eta + E_n - E_m} (f(E_n) - f(E_m)) \\
&+ \frac{[u_n^*(i+\hat{x})v_m^*(i) - u_n^*(i)v_m^*(i+\hat{x})]v_m(j)v_n(j)}{\omega + i\eta + E_n + E_m} (f(E_n) + f(E_m) - 1) \\
&- \frac{[v_n(i+\hat{x})u_m(i) - v_n(i)u_m(i+\hat{x})]u_m^*(j)u_n^*(j)}{\omega + i\eta - E_n - E_m} (1 - f(E_n) - f(E_m)) \\
&- \frac{[v_n(i+\hat{x})v_m^*(i) - v_n(i)v_m^*(i+\hat{x})]u_n^*(j)v_m(j)}{\omega + i\eta - E_n + E_m} (-f(E_n) + f(E_m))
\end{aligned} \tag{S8}$$

$$\begin{aligned}
\chi_{ij}(j^x, \delta n) = & 2it \sum_{nm} \frac{[u_n^*(i + \hat{x})u_m(i) - u_n^*(i)u_m(i + \hat{x})][u_m^*(j)u_n(j) - v_n(j)v_m^*(j)]}{\omega + i\eta + E_n - E_m} (f(E_n) - f(E_m)) \\
& + \frac{[u_n^*(i + \hat{x})v_m^*(i) - u_n^*(i)v_m^*(i + \hat{x})][v_m(j)u_n(j) + v_n(j)u_m(j)]}{\omega + i\eta + E_n + E_m} (f(E_n) + f(E_m) - 1) \\
& + \frac{[v_n(i + \hat{x})u_m(i) - v_n(i)u_m(i + \hat{x})][u_m^*(j)v_n^*(j) + u_n^*(j)v_m^*(j)]}{\omega + i\eta - E_n - E_m} (1 - f(E_n) - f(E_m)) \\
& + \frac{[v_n(i + \hat{x})v_m^*(i) - v_n(i)v_m^*(i + \hat{x})][v_m(j)v_n^*(j) - u_n^*(j)u_m(j)]}{\omega + i\eta - E_n + E_m} (-f(E_n) + f(E_m)) \quad (S9)
\end{aligned}$$

The correlation functions between the pair fluctuations ( $\delta\Delta$ ,  $\delta\Delta^\dagger$ ) and the density fluctuations ( $\delta n$ ) are given by,

$$\begin{aligned}
\chi_{ij}(\delta\Delta, \delta\Delta) = & \sum_{nm} -\frac{u_n(i)u_m(i)v_m^*(j)v_n^*(j)}{\omega + i\eta - E_n - E_m} (1 - f(E_n) - f(E_m)) + \frac{u_n(i)v_m^*(i)u_m(j)v_n^*(j)}{\omega + i\eta - E_n + E_m} (-f(E_n) + f(E_m)) \\
& + \frac{v_n^*(i)u_m(i)v_m^*(j)u_n(j)}{\omega + i\eta + E_n - E_m} (f(E_n) - f(E_m)) - \frac{v_n^*(i)v_m^*(i)u_m(j)u_n(j)}{\omega + i\eta + E_n + E_m} (f(E_n) + f(E_m) - 1) \quad (S10)
\end{aligned}$$

$$\begin{aligned}
\chi_{ij}(\delta\Delta, \delta\Delta^\dagger) = & \sum_{nm} \frac{u_n(i)u_m(i)u_m^*(j)u_n^*(j)}{\omega + i\eta - E_n - E_m} (1 - f(E_m) - f(E_n)) + \frac{u_n(i)v_m^*(i)v_m(j)u_n^*(j)}{\omega + i\eta - E_n + E_m} (-f(E_n) + f(E_m)) \\
& + \frac{v_n^*(i)u_m(i)u_m^*(j)v_n(j)}{\omega + i\eta + E_n - E_m} (f(E_n) - f(E_m)) + \frac{v_n^*(i)v_m^*(i)v_m(j)v_n(j)}{\omega + i\eta + E_n + E_m} (f(E_n) + f(E_m) - 1) \quad (S11)
\end{aligned}$$

$$\begin{aligned}
\chi_{ij}(\delta\Delta^\dagger, \delta\Delta) = & \sum_{nm} \frac{u_n^*(i)u_m^*(i)u_m(j)u_n(j)}{\omega + i\eta + E_n + E_m} (f(E_n) + f(E_n) - 1) + \frac{u_n^*(i)v_m(i)v_m^*(j)u_n(j)}{\omega + i\eta + E_n - E_m} (f(E_n) - f(E_m)) \\
& + \frac{v_n(i)u_m^*(i)u_m(j)v_n^*(j)}{\omega + i\eta - E_n + E_m} (-f(E_n) + f(E_m)) + \frac{v_n(i)v_m(i)v_m^*(j)v_n^*(j)}{\omega + i\eta - E_n - E_m} (1 - f(E_m) - f(E_n)) \quad (S12)
\end{aligned}$$

$$\begin{aligned}
\chi_{ij}(\delta n, \delta\Delta) = & 2 \sum_{nm} \frac{u_n^*(i)u_m(i)u_n(j)v_m^*(j)}{\omega + i\eta + E_n - E_m} (f(E_n) - f(E_m)) - \frac{u_n^*(i)v_m^*(i)u_m(j)u_n(j)}{\omega + i\eta + E_n + E_m} (f(E_n) + f(E_m) - 1) \\
& + \frac{v_n(i)u_m(i)v_m^*(j)v_n^*(j)}{\omega + i\eta - E_n - E_m} (1 - f(E_n) - f(E_m)) - \frac{v_n(i)v_m^*(i)v_n^*(j)u_m(j)}{\omega + i\eta - E_n + E_m} (-f(E_n) + f(E_m)) \quad (S13)
\end{aligned}$$

$$\begin{aligned}
\chi_{ij}(\delta n, \delta\Delta^\dagger) = & 2 \sum_{nm} \frac{u_n^*(i)u_m(i)u_m^*(j)v_n(j)}{\omega + i\eta + E_n - E_m} (f(E_n) - f(E_m)) + \frac{u_n^*(i)v_m^*(i)v_m(j)v_n(j)}{\omega + i\eta + E_n + E_m} (f(E_n) + f(E_m) - 1) \\
& - \frac{v_n(i)u_m(i)u_n^*(j)u_m^*(j)}{\omega + i\eta - E_n - E_m} (1 - f(E_n) - f(E_m)) - \frac{v_n(i)v_m^*(i)u_n^*(j)v_m(j)}{\omega + i\eta - E_n + E_m} (-f(E_n) + f(E_m)) \quad (S14)
\end{aligned}$$

$$\begin{aligned}
\chi_{ij}(\delta n, \delta n) = & 2 \sum_{nm} \frac{u_n^*(i)u_m(i)[u_m^*(j)u_n(j) - v_n(j)v_m^*(j)]}{\omega + i\eta + E_n - E_m} (f(E_n) - f(E_m)) + \frac{u_n^*(i)v_m^*(i)[v_m(j)u_n(j) + v_n(j)u_m(j)]}{\omega + i\eta + E_n + E_m} (f(E_n) + f(E_m) - 1) \\
& + \frac{v_n(i)u_m(i)[u_m^*(j)v_n^*(j) + u_n^*(j)v_m^*(j)]}{\omega + i\eta - E_n - E_m} (1 - f(E_n) - f(E_m)) + \frac{v_n(i)v_m^*(i)[v_m(j)v_n^*(j) - u_n^*(j)u_m(j)]}{\omega + i\eta - E_n + E_m} (-f(E_n) + f(E_m)) \quad (S15)
\end{aligned}$$

The remaining correlation functions (which we have not shown above) can be obtained by using the following symmetries,

$$\chi_{ij}(j^x, \delta\Delta^\dagger) = -\chi_{ji}(\delta\Delta, j^x) \quad (S16)$$

$$\chi_{ij}(j^x, \delta\Delta) = -\chi_{ji}(\delta\Delta^\dagger, j^x) \quad (S17)$$

$$\chi_{ij}(\delta\Delta^\dagger, \delta\Delta^\dagger) = \chi_{ji}(\delta\Delta, \delta\Delta) \quad (\text{S18})$$

$$\chi_{ij}(\delta\Delta^\dagger, \delta n) = \chi_{ji}(\delta n, \delta\Delta) \quad (\text{S19})$$

$$\chi_{ij}(\delta n, \delta\Delta^\dagger) = \chi_{ji}(\delta\Delta, \delta n). \quad (\text{S20})$$

Note that all the correlation functions reduce to the expressions provided in Ref. [33] in the limit  $T \rightarrow 0$ . Now, we express, using Eq. (S5), the different correlation functions in terms of the amplitude, phase and density fluctuations,

$$\chi_{ij}(j^x, A) = \frac{1}{\sqrt{2}} (\chi_{ij}(j^x, \delta\Delta) + \chi_{ij}(j^x, \delta\Delta^\dagger)) \quad (\text{S21})$$

$$\chi_{ij}(A, j^x) = \frac{1}{\sqrt{2}} (\chi_{ij}(\delta\Delta, j^x) + \chi_{ij}(\delta\Delta^\dagger, j^x)) \quad (\text{S22})$$

$$\chi_{ij}(j^x, \Phi) = \frac{i}{\sqrt{2}} (\chi_{ij}(j^x, \delta\Delta) - \chi_{ij}(j^x, \delta\Delta^\dagger)) \quad (\text{S23})$$

$$\chi_{ij}(\Phi, j^x) = \frac{i}{\sqrt{2}} (\chi_{ij}(\delta\Delta, j^x) - \chi_{ij}(\delta\Delta^\dagger, j^x)) \quad (\text{S24})$$

$$\chi_{ij}(A, A) = \frac{1}{2} [\chi_{ij}(\delta\Delta, \delta\Delta) + \chi_{ij}(\delta\Delta, \delta\Delta^\dagger) + \chi_{ij}(\delta\Delta^\dagger, \delta\Delta) + \chi_{ij}(\delta\Delta^\dagger, \delta\Delta^\dagger)] \quad (\text{S25})$$

$$\chi_{ij}(A, \Phi) = \frac{i}{2} [\chi_{ij}(\delta\Delta, \delta\Delta) - \chi_{ij}(\delta\Delta, \delta\Delta^\dagger) + \chi_{ij}(\delta\Delta^\dagger, \delta\Delta) - \chi_{ij}(\delta\Delta^\dagger, \delta\Delta^\dagger)] \quad (\text{S26})$$

$$\chi_{ij}(A, \delta n) = \frac{1}{\sqrt{2}} [\chi_{ij}(\delta\Delta, \delta n) + \chi_{ij}(\delta\Delta^\dagger, \delta n)] \quad (\text{S27})$$

$$\chi_{ij}(\Phi, A) = \frac{i}{2} [\chi_{ij}(\delta\Delta, \delta\Delta) + \chi_{ij}(\delta\Delta, \delta\Delta^\dagger) - \chi_{ij}(\delta\Delta^\dagger, \delta\Delta) - \chi_{ij}(\delta\Delta^\dagger, \delta\Delta^\dagger)] \quad (\text{S28})$$

$$\chi_{ij}(\Phi, \Phi) = \frac{i^2}{2} [\chi_{ij}(\delta\Delta, \delta\Delta) - \chi_{ij}(\delta\Delta, \delta\Delta^\dagger) - \chi_{ij}(\delta\Delta^\dagger, \delta\Delta) + \chi_{ij}(\delta\Delta^\dagger, \delta\Delta^\dagger)] \quad (\text{S29})$$

$$\chi_{ij}(\Phi, \delta n) = \frac{i}{\sqrt{2}} [\chi_{ij}(\delta\Delta, \delta n) - \chi_{ij}(\delta\Delta^\dagger, \delta n)] \quad (\text{S30})$$

$$\chi_{ij}(\delta n, A) = \frac{1}{\sqrt{2}} [\chi_{ij}(\delta n, \delta\Delta) + \chi_{ij}(\delta n, \delta\Delta^\dagger)] \quad (\text{S31})$$

$$\chi_{ij}(\delta n, \Phi) = \frac{i}{\sqrt{2}} [\chi_{ij}(\delta n, \delta\Delta) - \chi_{ij}(\delta n, \delta\Delta^\dagger)] \quad (\text{S32})$$

The above expressions are predictions for the different susceptibilities. Ultimately, our main focus is to calculate the current-current correlation functions that enter in the definition of the conductivity. However, it is necessary to compute the current-current correlations beyond the mean-field limit so our results are gauge invariant and can reproduce collective excitations that may impact the performance of the superinductor device. In order to proceed, we compute these corrections within the random phase approximation [25] that allows us to express them in terms of the susceptibilities above. Diagrammatically, these deviations correspond to vertex corrections to the mean-field bubble-diagrams representing the bare current-current correlation function. The full gauge invariant current-current correlation function is given by [29, 30, 33],

$$\chi_{ij}(j^x, j^x) = \chi_{ij}^0(j^x, j^x) + \Lambda_{ip} \mathbb{V}_{pl} (\mathbb{I}_{3N \times 3N} - \chi^B \mathbb{V})_{ls}^{-1} \bar{\Lambda}_{sj} \quad (\text{S33})$$

where  $\chi^0$  is the bare current-current correlation function (S6), and  $\Lambda$  is a matrix whose entries are the susceptibilities above of the current with the amplitude fluctuations  $A$ , phase fluctuations  $\Phi$  or charge density fluctuations  $\delta n$ ,

$$\Lambda = (\chi(j^x, A) \quad \chi(j^x, \Phi) \quad \chi(j^x, \delta n)) \quad (\text{S34})$$

$$\bar{\Lambda} = (\chi(A, j^x) \quad \chi(\Phi, j^x) \quad \chi(\delta n, j^x))^T. \quad (\text{S35})$$

$\chi^B$  is the bare mean-field susceptibility and  $\mathbb{V}$  is the effective local interaction, defined by  $3 \times 3$  matrices in the basis of fluctuations.

$$\chi^B = \begin{pmatrix} \chi^{AA} & \chi^{A\Phi} & \chi^{A\delta n} \\ \chi^{\Phi A} & \chi^{\Phi\Phi} & \chi^{\Phi\delta n} \\ \chi^{\delta n A} & \chi^{\delta n\Phi} & \chi^{\delta n\delta n} \end{pmatrix} \quad (\text{S36})$$

and

$$\mathbb{V} = \begin{pmatrix} -|U| & 0 & 0 \\ 0 & -|U| & 0 \\ 0 & 0 & -|U|/2 \end{pmatrix} \quad (\text{S37})$$

For example, in Eq. (S33),  $\chi^B(A, A) = \chi^{AA}$ ,  $\mathbb{V}^A = -|U|\mathbb{I}_{N \times N}$ . Note that all of these correlation function are  $N \times N$  matrices in real space.

The complex optical conductivity  $\sigma(\omega) = \sigma_1(\omega) - i\sigma_2(\omega)$  is obtained [29–31, 81] directly from the susceptibility  $\chi(\omega)$ ,

$$\sigma_1(\omega) = \pi D_s \delta(\omega) + e^2 \text{Im} \frac{\chi(\omega)}{\omega} \quad (\text{S38})$$

$$\sigma_2(\omega) = e^2 \frac{\langle -k_x \rangle + \text{Re} \chi(\omega)}{\omega} \quad (\text{S39})$$

where  $\text{Im}$  stands for the imaginary part of  $\chi(\omega) = 1/N \sum_{ij} \chi_{ij}(j^x, j^x)$ , while  $\text{Re}$  is the real part.  $e$  is the elementary charge,  $D_s = e^2[\langle -k_x \rangle + \text{Re} \chi(\omega = 0)]$  is the superfluid stiffness, and  $\langle -k_x \rangle = \frac{4t}{N} \sum_i \sum_n [u_n(i)u_n(i+x)f(E_n) + v_n(i)v_n(i+x)(1 - f(E_n))]$  is the kinetic energy along the  $x$  direction.

The quality factor of a transmission line is defined as [63]  $Q = \frac{\alpha}{2\beta}$ , where  $\alpha$  and  $\beta$  are the real and imaginary parts of the propagation constant  $\gamma$ . The superinductor which absorbs electromagnetic radiation can be treated as a lossy media. Therefore, the complex propagation constant of the plane wave can be written as [62, 64]

$$\gamma = \sqrt{i\omega\mu(\sigma + i\omega\epsilon)} = \alpha + i\beta, \quad (\text{S40})$$

where  $\epsilon$  and  $\mu$  are the permittivity and permeability of the media, respectively. With the assumption  $\sigma_2 \gg \sigma_1$ , one can easily obtain

$$\begin{aligned} Q &= \frac{\alpha}{2\beta} \\ &= \frac{\cos\left(\frac{\arctan \frac{\sigma_1}{\sigma_2 - 2\pi f \epsilon}}{2}\right)}{2 \sin\left(\frac{\arctan \frac{\sigma_1}{\sigma_2 - 2\pi f \epsilon}}{2}\right)} \\ &\approx \frac{\sigma_2}{\sigma_1}. \end{aligned} \quad (\text{S41})$$

Likewise, the kinetic inductance is also expressed in terms of the complex conductivity  $L_{k/\square} = \frac{1}{2\pi f \sigma_2}$  [75, 82].

### ESTIMATION OF FINITE SIZE EFFECTS

Due to the limitation of our computational resources, the maximum size we could reach is  $N = L \times L = 32 \times 32$ . For this size, there are strong size effects for  $V = 0$ , no disorder, because the coherence length  $\xi$  is much larger than the system size in the weak-coupling limit of interest. We expect that as  $V$  increases, the coherence length decreases and finite size effects will become negligible. In Fig. S1, we show the size dependence of the spatial averaged order parameter  $\langle \Delta \rangle$  and spectral gap  $E_g$ , the quality factor  $Q$ , and the kinetic inductance  $L_{k/\square}$  for  $V = 1.5$ . The size dependence is quite weak when  $L \geq 26$ , so finite size effects are not important in the region close to the transition  $V \gtrsim 1.5$  which is the main focus of the paper.



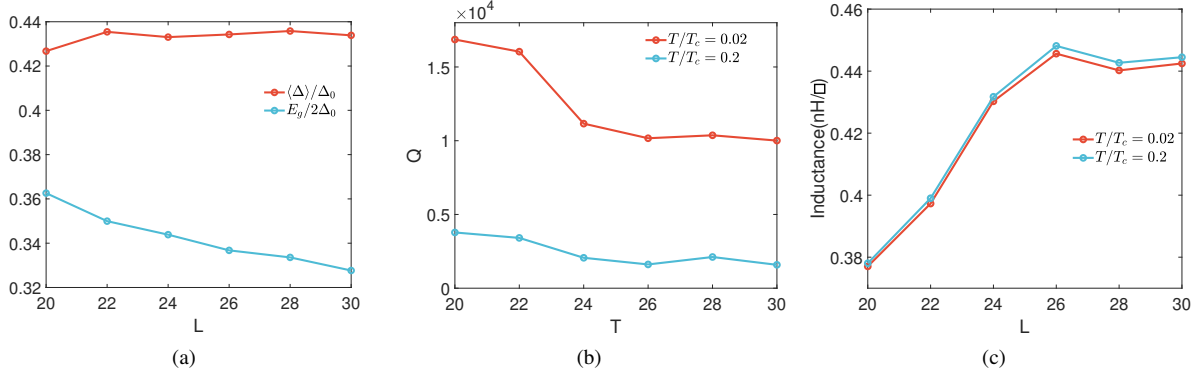


Figure S1. (a). The spatial averaged order parameter  $\langle \Delta \rangle$  and the spectral gap  $E_g$ , normalized by factors of  $\Delta_0$ . It is evident that  $\langle \Delta \rangle$  changes only slightly with size. (b) The Quality factor  $Q$  and (c) kinetic inductance  $L_k / \square$ . The disorder is  $V = 1.5$ , and the frequency is  $f = 0.112\Delta_0$ . The other parameters are  $U = -1$ ,  $\langle n \rangle = 0.875$ . We do not observe any substantial size dependence in  $Q$  or  $L_k / \square$ , when  $L \geq 26$  at  $V = 1.5$ . For stronger coupling or disorder strength, finite size effects will be even smaller.

### THE QUALITY FACTOR COMPUTED FROM THE SAMPLE-AVERAGED CONDUCTIVITY

In the main text, the quality factor  $Q$  was computed from the sample-averaged conductivity, namely, we compute the conductivity for each disorder realization, then we perform the average over all disorder realizations. Finally, the quality factor was obtained from this averaged quantity. This is justified because our system size is small compared to the experimental one. Note that assuming a lattice spacing of 0.35nm, our typical lattice size is 10 nm  $\times$  10 nm.

For a single configuration of the conductivity, since the size is not large enough, we might get some spurious sub-gap excitation peaks which would lead to huge sample-sample variations in the quality factor. In experiments, since the sample size is much larger, it can access all possible excitations within a single sample. Therefore, by first performing the average of the conductivity, we reduce significantly the statistical error. In Fig. S2, we depict the quality factor for all disorder values we have studied. As in the main text, the sample-average of the conductivity was carried out first, We shall see in next section that these results are consistent with those obtained by computing the quality factor for each disorder realization and then performing the ensemble average over all disorder realizations.

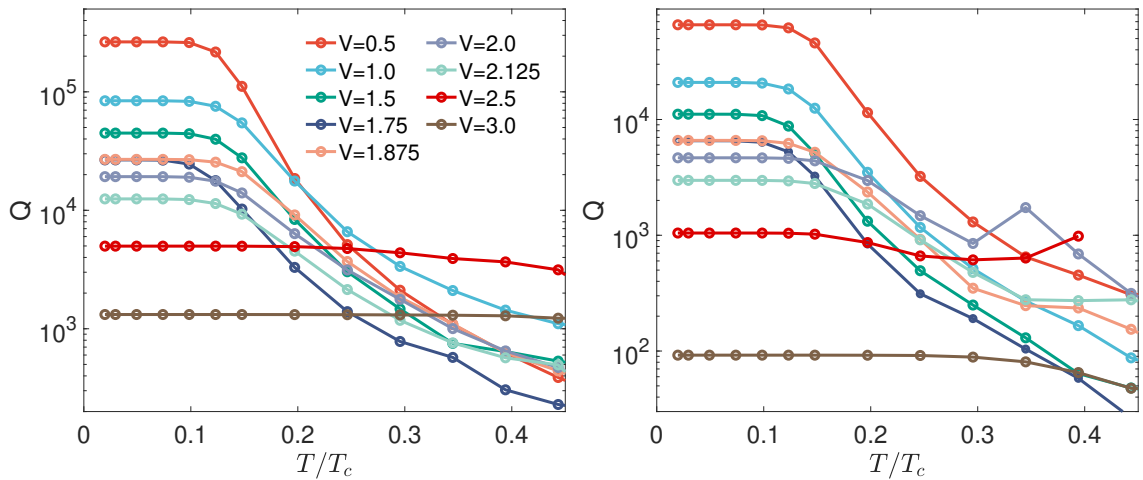


Figure S2. Quality factor as a function of temperature for different disorder strength  $V$  with sample-averaged conductivity. The frequencies are  $f = 0.028\Delta_0$  (left panel) and  $f = 0.112\Delta_0$  (right panel). Other parameters are  $N = 28 \times 28$ ,  $U = -1$ ,  $\langle n \rangle = 0.875$ .

### THE SAMPLE AVERAGED QUALITY FACTOR AND KINETIC INDUCTANCE

In this section, we present results of the sample-averaged quality factor  $Q$  and kinetic inductance  $L_{k/\square}$ . By sample-average, we mean that, unlike the previous two sections, we compute  $Q$  and  $L_{k/\square}$  for each disorder realization and, after that, we perform the ensemble average. In Fig. S3, we depict the size dependence of  $Q$  and  $L_{k/\square}$  as a function of the system size. These results are very similar to those of Fig. S1 where  $Q$  and  $L_{k/\square}$  were computed by first carrying out the disorder average of the conductivity.

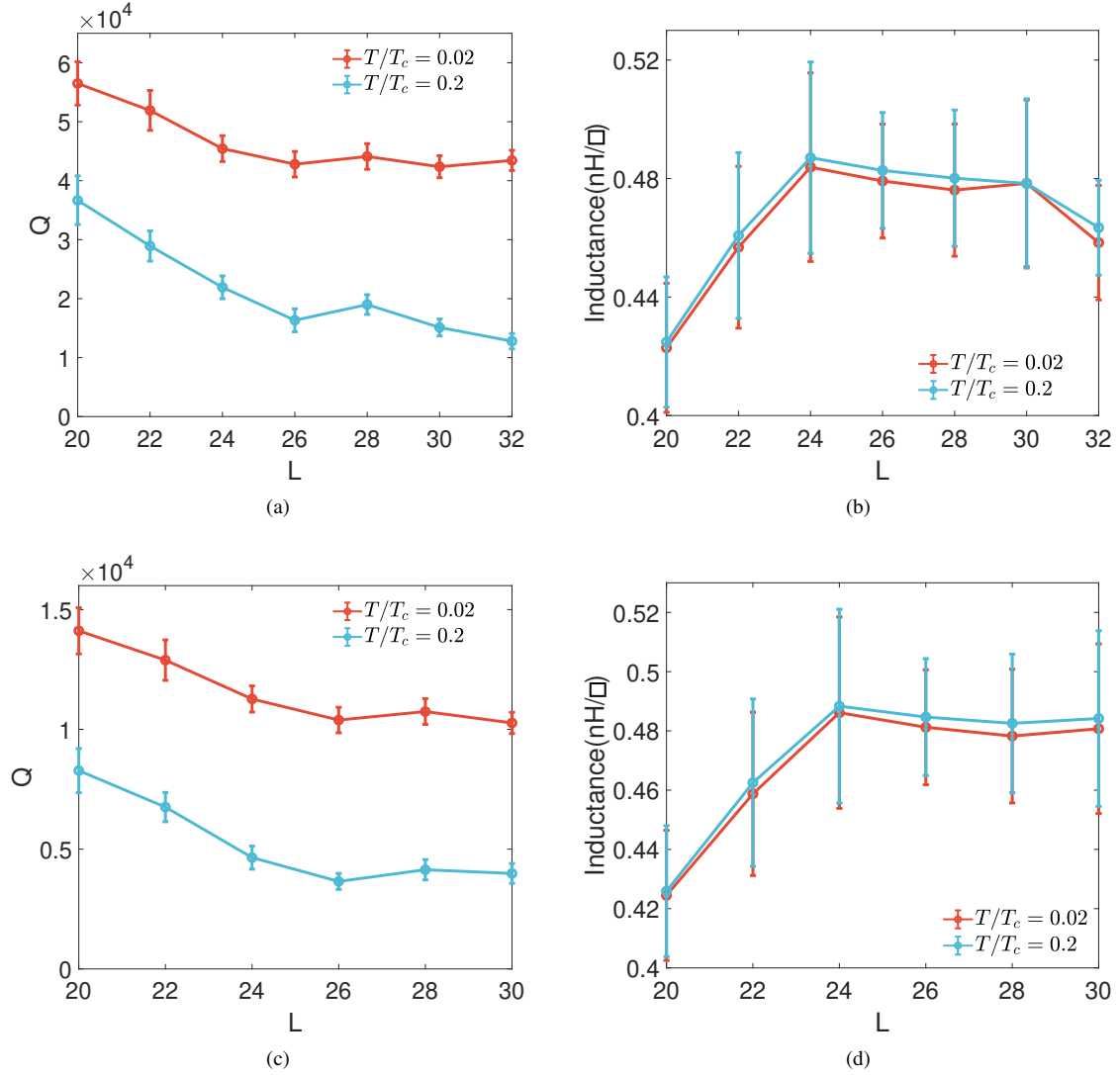


Figure S3. The Quality factor  $Q$  (left) and kinetic inductance  $L_{k/\square}$  (right) as a function of system size. The disorder is  $V = 1.5$  and the frequencies are  $f = 0.028\Delta_0$  (top row) and  $f = 0.112\Delta_0$  (bottom row). Other parameters are the same as those of Fig. S1. Here, we have done the sample averaging in the final step while calculating  $Q$  and  $L_{k/\square}$ . Notice that the results are consistent with Fig. S1.

Next we compute  $Q$  as a function of the temperature for different values of the disorder strength. If there are enough disorder realizations, the quality factor  $Q$  computed by averaging over disorder, see Fig. S4, is almost identical than the one performing first the average over the conductivity and then computing the quality factor, see Fig. S2. The exponential increase of the kinetic inductance  $L_{k/\square}$ , see Fig. S5, is also observed by this approach with results consistent with those presented in the main text.

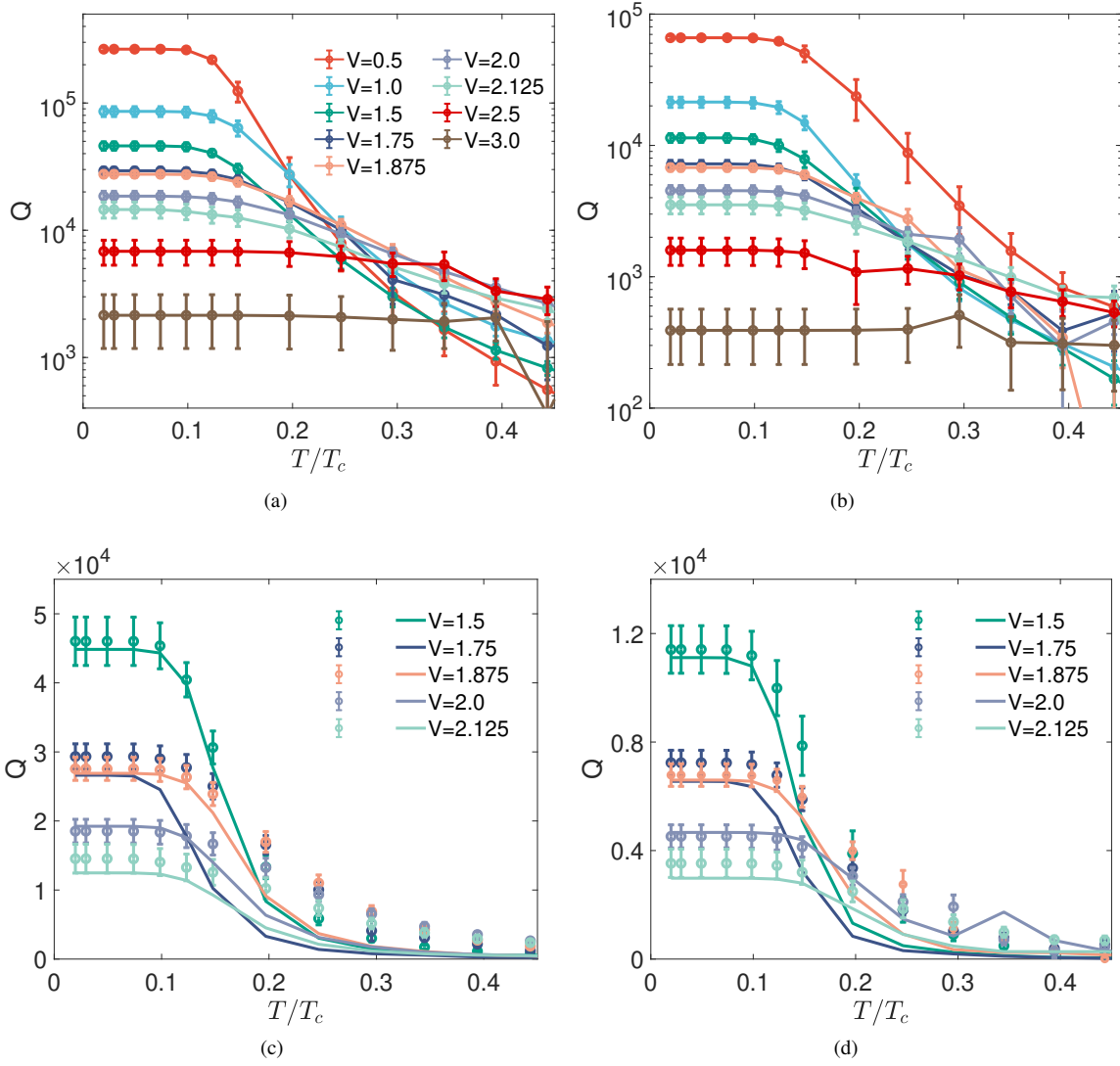


Figure S4. Quality factor as a function of temperature for different disorder strength for a lattice  $N = 28 \times 28$ ,  $U = -1$ ,  $\langle n \rangle = 0.875$ . The frequency for (a) is  $f = 0.028\Delta_0$ , and for (b) is  $f = 0.112\Delta_0$ . The lower panel includes the same plots with above but in linear scale, and only around the critical disorder. The sample averaged quality factors are presented by the circles with error bar, and the solid lines are the corresponding results based on sample averaged conductivity results. The deviations between two methods are small. In the clean limits, we have  $\Delta_0 = 0.0357t$ ,  $T_c \approx 0.02t$  based on the BCS assumption.

### THE QUALITY FACTOR FOR A CAVITY RESONATOR

Based on the prediction of high frequency dissipation in a superconducting cavity, the quality factor is given by [75]

$$Q = \frac{f}{2c} \frac{\mathcal{V}}{S} \frac{\pi \left( \frac{\sigma_2}{4\pi\epsilon} \right)^2}{\frac{\sigma_1}{4\pi\epsilon} \sqrt{2\pi f \left( \left| \frac{\sigma}{4\pi\epsilon} \right| + \frac{\sigma_2}{4\pi\epsilon} \right)}} \approx \frac{\pi \left( \frac{\sigma_2}{4\pi\epsilon} \right)^2}{2 \frac{\sigma_1}{4\pi\epsilon} \sqrt{2\pi f \left( \left| \frac{\sigma}{4\pi\epsilon} \right| + \frac{\sigma_2}{4\pi\epsilon} \right)}}, \quad (\text{S42})$$

where  $c$  is the speed of light,  $\mathcal{V}$  is the volume of the superconductor cavity and  $S$  is the corresponding surface area. For the sake of clarity, we use the conventional symbol  $f$  for the frequency to replace  $\omega$ . Here, we are assuming that the superconductor cavity is operating at the lowest modes, so that the typical linear dimension of the cavity  $l = \frac{\mathcal{V}}{S}$  is of the order of the radiation wavelength  $\lambda = c/f$ .

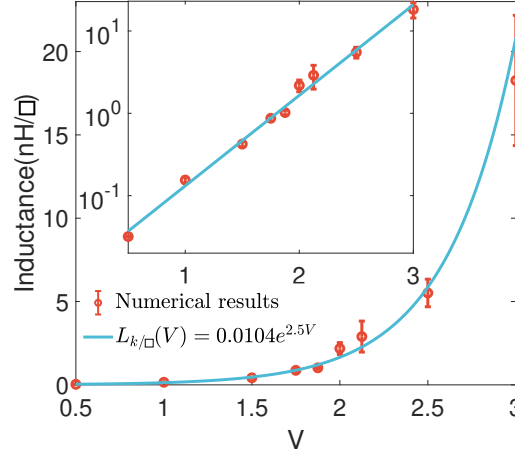


Figure S5. The kinetic inductance  $L_k$  as a function of disorder  $V$ . The numerical results fits well with an exponential increase of  $L_k$  with disorder. The fitting exponent is 2.5, which is consistent with the result 2.3 in the main text. The other parameters are  $N = 28 \times 28$ ,  $U = -1$ ,  $\langle n \rangle = 0.875$ .

In the limit of  $\sigma_2 \gg \sigma_1$ , Eq.(S42) can be approximated by

$$Q \approx \sqrt{\frac{\pi}{4}} \sqrt{\frac{\sigma_2}{4\pi f \epsilon}} \frac{\sigma_2}{\sigma_1}. \quad (\text{S43})$$

It has been shown [63] that in a microwave resonator, the working frequency of the superinductor, which is near the resonate frequency  $f$ , is proportional to  $\sigma_2$ . Therefore, comparing Eqs. (S41) and (S43), the quality factor in the cavity case should qualitatively agree with the planar case, up to a prefactor  $\sqrt{\frac{\pi}{4}} \sqrt{\frac{\sigma_2}{4\pi f \epsilon}}$  which only depends weakly on disorder and temperature.

The quality factor, see Figs. S6 and S7, is computed using Eq. (S42). Although the value of  $Q$  is significantly larger than that in the micro-stripe geometry studied in the main text, the temperature and disorder dependence are very similar. This is expected because the dependence on temperature and disorder is largely controlled only by  $1/\sigma_1$  [63] and  $Q \propto 1/\sigma_1$  in both cases. Therefore, based on those numerical results, we expect that the main findings of the paper apply to the experiments on both planar resonators and cavities, though the numerical values of  $Q$  will be different.

## THE ESTIMATION OF CRITICAL DISORDER BY PERCOLATION AND THE ENERGY GAP

In this section, we estimate the critical disorder  $V = V_c$  at which the transition occurs in order to determine whether the disorder strength  $V \simeq 1.875$  for an optimal operation of the superinducting device is still on the metallic side of the transition. For that purpose, we carry out a percolation analysis [83] based on the site-dependent amplitude of the superconducting order parameter  $\Delta(r)$ . We compute the maximum disorder strength  $V$  for which a percolating cluster exist.

Strictly speaking, this is controlled by the probability  $p$  that a given site has a finite value. In a simple 2D lattice, the percolating transition occurs for  $p_c = 0.59$  [84]. In our case, we get finite values of  $\Delta(i)$  for every site. However, we expect that if the order parameter is very small with respect to the clean value, it will not be able to carry a supercurrent because phase fluctuation will prevent local phase coherence. For that reason, we perform the percolation analysis with a cut-off value  $\Delta_c$  of the order parameter, namely, we consider that a site belongs to the cluster only if  $\Delta > \Delta_c$ . Results depicted in Fig. 8(a) predict a critical disorder, which is relatively sensitive to the cutoff, of about  $V \simeq 2$ . Another way to estimate the location of the transition is by computing the spectral gap as a function of the disorder strength. It is expected that it will decrease with disorder for weak disorder but this trend is reversed around the transition due to Anderson localization effects [65]. The estimation of the critical disorder,  $V = 1.75$ , by this method, see Fig. 8(b), is consistent with the percolation calculation. Therefore, given the uncertainties of this estimates, the optimal disorder  $V \simeq 1.875$  for the operation of the superinductor device seem to fall on the critical region but clearly not on the insulating side.



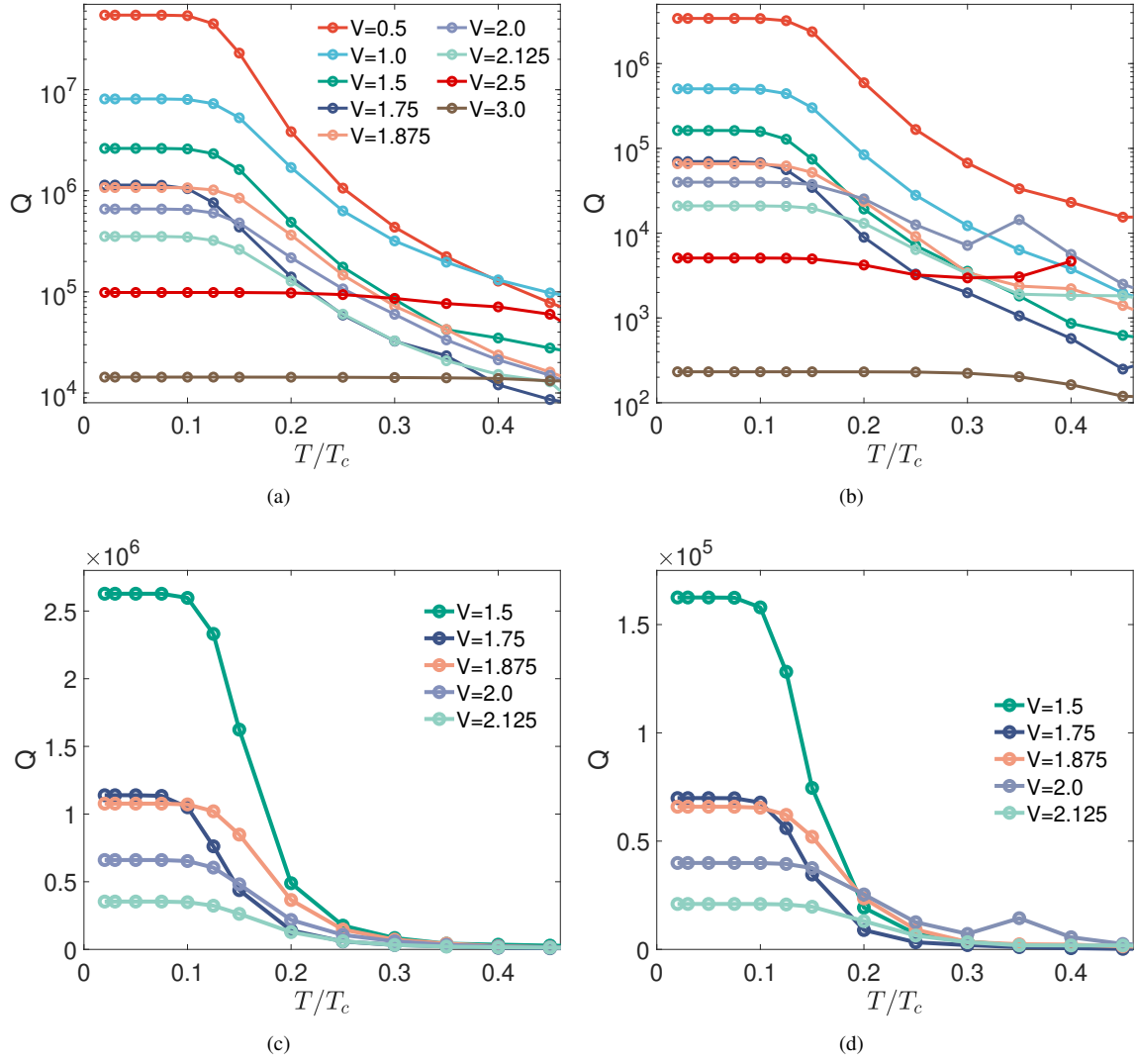


Figure S6. Quality factor  $Q$  as a function of temperature for different disorder strength for a lattice  $N = 28 \times 28$ ,  $U = -1$ ,  $\langle n \rangle = 0.875$ . The frequency for (a) is  $f = 0.028\Delta_0$ , and for (b) is  $f = 0.112\Delta_0$ . The lower panel contains the same information but in linear scale, and only around the critical disorder. The quality factor are calculated by using Eq.(S42) based on sample averaged conductivity results.

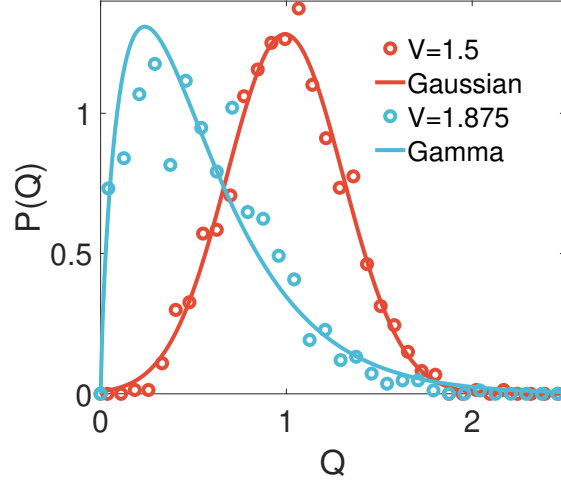


Figure S7. Probability distribution of  $Q$  from 1000 disorder realizations, normalized by the average of  $Q(V = 1.5) \sim 2.5 \times 10^6$  for  $f = 0.028\Delta_0 \sim 2.5$  GHz, and temperature  $T/T_c = 0.05$ . When  $V = 1.5$ , the distribution of  $Q$  fits well with a Gaussian distribution, red line. However, very close to the transition  $V \approx 1.9 \approx V_c$ , the distribution, asymmetric and with broad tails, is similar to a Gamma distribution (blue line). The results are similar to those of the planar case presented in the main text.

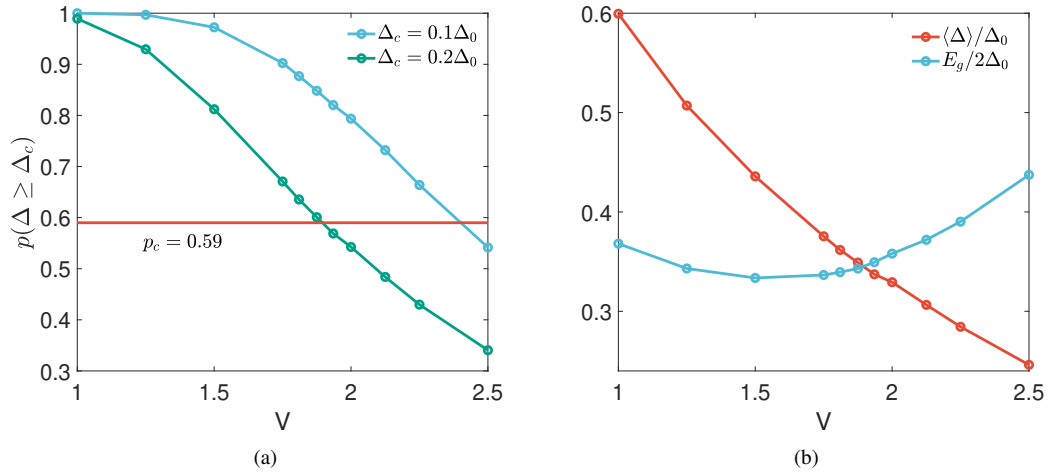


Figure S8. (a). The probability of  $\Delta(r) \geq \Delta_c$ . In order to estimate the location of the transition, we show results for two cut-off values  $\Delta_c = 0.1\Delta_0$  and  $0.2\Delta_0$ . The red line is the percolation threshold  $p_c = 0.59$  for a simple 2D square lattice [84]. Based on the percolation results, the transition disorder is around  $V = 2$ . (b). The spatial average of the order parameter  $\langle \Delta \rangle$  (normalized by  $\Delta_0$ ) and mean value of the spectral gap  $E_g$  (normalized by  $2\Delta_0$ ). As expected, the spatial averaged order parameter  $\langle \Delta \rangle / \Delta_0$  decreases monotonously with disorder, and the spectral gap  $E_g / 2\Delta_0$  decreases with disorder first and then increases around  $V = 1.75$ . The transition is expected to occur at this minimum of the spectral gap. To reduce statistical error, we calculate 2000 disorder realizations for each  $V$ .